Hindawi
Advances in Materials Science and Engineering
Volume 2018, Article ID 7982396, 10 pages
https://doi.org/10.1155/2018/7982396

Research Article

Compression Behavior of Basalt Fiber-Reinforced Polymer Tube-Confined Coconut Fiber-Reinforced Concrete

Yang Lv, Xueqian Wu, Yuhao Zhu, Xiao Liang, Quanxi Cheng, and Mengran Gao

Tianjin Key Laboratory of Civil Structure Protection and Reinforcement, Tianjin Chengjian University, Tianjin 300384, China

Correspondence should be addressed to Yang Lv; lvyangtju@163.com

Received 22 April 2018; Revised 21 June 2018; Accepted 12 August 2018; Published 12 September 2018

Academic Editor: Guoqiang Xie

Basalt fiber is cheap and has excellent mechanical performance. In addition, in combination with the environmentally friendly coconut fiber, it can contribute to sustainable construction materials. In this study, a composite material consists of basalt fiber-reinforced polymer (BFRP) tube-encased coconut fiber-reinforced concrete (CFRC) is developed. The 28-day compression strength of the plain concrete is about 15 MPa, which represents the low strength and poor-quality concrete widely existing in a large number of old buildings. The concrete was poured and cured into the steel moulds, BFRP tubes with the inner diameter of 100 mm and a height of 200 mm, and BFRP tubes with the inner diameter of 160 mm and a height of 320 mm, respectively. In total, 36 cylindrical specimens were constructed and tested. The axial compression tests were carried out to examine the strength and ductility enhancement due to the confinement of the BFRP tubes and coconut fibers. Also, the existing models were used to predict the ultimate axial compression strength and strain. The results show that the size of the specimen significantly influences the predicted compression strength.

1. Introduction

Over the last decades, engineers are more aware of the environment and the limited resource, which has promoted the usage of natural fibers in polymer reinforcement. A huge number of natural fibers like sisal, kenaf, hem, flax, coconut, bamboo, and banana have been studied. Among these natural fibers, coconut fibers have gained popularity because of the cost-effective and high mechanical properties compared with other fibers, for example, bamboo or flax fibers [1]. Coconut fiber is extracted from the outer shell of coconut. More than 500,000 tons of coconut fibers were produced annually worldwide. Reis [2] reported that coconut fibers increased the fracture toughness of concrete composite. The coconut fibers even showed a better flexural property than that of glass and carbon fibers. Baruah and Talukdar [3] reported that the compressive, tensile, and shear strengths of coconut fiber-reinforced concrete (CFRC) increased about 13.7%, 22.9%, and 32.7% compared with those of plain concrete (PC), respectively. CFRC specimens remain intact due to the bridging effect of coconut fibers following a splitting test. Islam et al. [4] found that the addition of 0.5% coconut fibers by volume enhanced the flexural strength of normal concrete and high-strength concrete composite by 60% and 6%, respectively. Their research also indicated that the ductility and toughness of both normal- and high-strength concrete increased with a larger volume fraction content of coconut fibers. Hasan et al. [5] studied the lightweight concrete structure using coconut fibers as reinforcement. Ali et al. [6] examined the effects of coconut fiber lengths and fiber contents on the mechanical properties of concrete.

To overcome possible shortcomings of fibers, fibers can be embedded in a polymer matrix to fabricate a composite called fiber-reinforced polymer (FRP). The most popularly used high-strength fibers are carbon fiber, glass fiber, and basalt fiber. In comparison to other fibers, basalt fiber has superior characteristics, that is, high strength to weight ratio, excellent ductility and durability, high thermal resistance, good corrosion resistance, and cost-effectiveness, and it has been investigated for decades by a number of researchers [7–13]. Basalt fiber-reinforced polymer (BFRP) composite

has also been employed in practice, for example, for post-earthquake rehabilitation and strengthening. Lopresto et al. [14] studied the mechanical properties of BFRP and glass FRP (GFRP) composites. Their results show that BFRP has a higher Young's modulus, compressive and bending strength, higher impact force resistance, and energy absorption capacity than GFRP. Wu et al. [15] investigated the tensile properties of basalt fibers and epoxy composites in corrosive environment. They found that the failure at the interface between the fibers and the resin governs the fracture properties of BFRP. They [16] also studied the fatigue behavior of different fiber-reinforced polymers made of carbon, glass, basalt, and hybrid fibers. The results have shown that the tensile modulus of the fiber affects the failure modes of composite coupons. Colombo et al. [17] investigated the static properties of BFRP, manufactured by vacuum infusion process and hand layup process. They also investigated the mechanical properties of different polymer matrices. Chen et al. [18] examined the quasi-static and dynamic tensile properties of BFRP. They found that the tensile strength, failure strain, and elastic modulus increase rapidly with the strain rate.

In this work, two sizes of BFRP tubes, that is, one with the inner diameter of 100 mm and height of 200 mm and the other with the inner diameter of 160 mm and height of 320 mm, were fabricated using a hand layout process. In total, 36 specimens were poured and cured in the steel moulds and 2-layer and 4-layer BFRP tubes, respectively. Compressive tests were carried out to investigate the enhancement of strength and ductility due to the confinement of BFRP tube and an inclusion of coconut fibers in the concrete. The results are compared with those obtained from analytical confinement models and discussed.

2. Experiments

2.1. BFRP Tube Fabrication. Commercial bidirectional woven basalt fabric (300 g/m^2) was used. The fabric has a plain woven structure with a count of 5.5 threads/cm in both warp and weft directions. The epoxy was Hoxion 35C resin and hardener. The woven basalt fabric was wrapped around the PVC tube using a hand layup process. After 24 hours curing in room temperature, the tubes were demoulded and put into an oven for 8 hours with a constant temperature of 80°C to increase the hardening. The weft direction of the fabric was aligned parallel to the axis of the tube. There were two groups of tubes. One group each had an inner diameter of 100 mm and length of 200 mm. The other group each had an inner diameter of 160 mm and height of 320 mm. The tubes were made of two and four layers of basalt fabrics. Figure 1 displays the BFRP tubes preparation prior to concrete casting.

9 coupons were fabricated and cured in the same condition with the BFRP tubes and the coupons were tested on a universal testing machine. Figure 2 shows the stress-strain relationship of the coupons of 2-layer, 4-layer, and 6-layer. The modulus of the BFRP is between 13.5 and 15.0 GPa.

2.2. BFRP-CFRC Composite. The coconut fiber had been roughly pretreated and cut to lengths of about 50 mm. The coconut fiber content was 1% of the cement mass. Two batches of concrete without and with coir were prepared. Both batches were designed as PC with a 28-day compression strength of 15 MPa to represent the low-strength concrete. In the second batch, coconut fiber was added. The concrete mix ratio by mass was 1:0.58:3.72:2.37:0.00245 for cement: water: gravel: sand: water reducer, respectively. The cement used was 32.5 normal Portland cement. The gravel has a maximum size of 25 mm. The natural sand was used as fine aggregate with a fineness modulus of 2.75. The matrix of the specimens prepared for this study consists of 36 cylindrical specimens and the test matrix of the specimens was given in Table 1.

2.3. Axial Compression Test. For compression tests, four strain gauges were used for each cylinder. Two strain gauges were mounted at the midheight of a cylinder aligned along the hoop direction to measure the hoop strain, and two strain gauges were mounted and aligned along the axial compressive direction to measure the axial strain. Two linear variable transducers (LVDTs) were installed between the two surfaces of the compressive machine. Figure 3 shows the compressive test setup of a PC specimen. Each specimen was axially compressed up to failure. Readings of the stain gauges, LVDT, and load cell were taken by a data logging system.

3. Results and Discussion

3.1. Stress-Strain Relationship. Figures 4–7 show the stress-strain curves of the small-size PC and CFRC specimens, the large-size PC and CFRC specimens, respectively. For the small-size specimens, the stress-strain curves can be divided into three regions [19], that is, the linear region, the microcracks-formed region, and the region of activated confinement. In the first region, the stress-strain behavior of the confined specimen is similar to that of the PC and CFRC specimens. The stress increases linearly with the axial strain. There is little lateral expansion of the PC and CFRC core, and the confinement of BFRP tube is not yet activated. When the stress approaches the peak strength of the PC and CFRC, the curves enter the nonlinear transition region. The microcracks begin to propagate in concrete. The lateral expansion gradually increases, and the PC and CFRC specimens are suddenly crushed and lost the axial load-bearing capacity at last. However, for the BFRP tube-confined PC and CFRC specimens, the lateral expansion is impeded by the lateral confinement of the BFRP tube and the stiffness gradually decreases with the axial strain. In the third region, the confinement of the BFRP tube is fully activated, and the stress of the confined specimens increases linearly with the axial strain. The compressive strength and ductility of the confined specimens increase significantly compared with those of PC and CFRC specimens. Meanwhile, the confined stress of the BFRP tube in the hoop direction increases simultaneously with the expansion of the concrete core.

(a) (b) (c)

Figure 1: BFRP tubes preparation. BFRP tubes (a, b) without CFRC and (c) with CFRC.

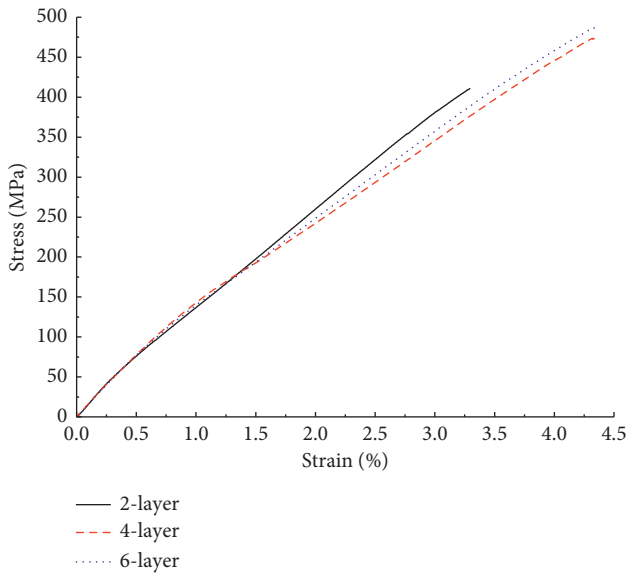

Figure 2: Effect of the number of layers on stress-strain relationship of BFRP-CFRC composites.

Once the hoop stress exceeds the tensile strength of BFRP, the specimen is suddenly crushed with a loud noise.

In the case of large-size specimens, the microcrack region is not obvious. In the third region, the stiffness is greatly reduced because of the weaker confinement compared with the small-size specimens (the confinement ratio is 160 : 100 for the small-size specimen to the large-size specimen). The difference between PC and CFRC strength is not significant. The ductility of the CFRC specimens are better than that of the PC ones. However, the ultimate compressive strength of the large-size specimen is smaller than that of the small-size one, owing to the weaker confinement of the BFRP tube as mentioned earlier.

3.2. Confinement Analysis. The average compression strengths of the specimens are listed in Table 2. f'_{c0} and ε_{c0} are, respectively, the peak compressive strength and axial strain of the unconfined concrete. f'_{cc} and ε_{cc} are, respectively, the ultimate compressive strength and ultimate strain of the confined concrete. ε_{hoop} is the rupture strain of the BFRP tube in the hoop direction. f_l is the lateral confining pressure produced by the BFRP tube in the hoop direction. f'_{cc}/f'_{c0} is the confinement effectiveness. f_l/f'_{c0} is the ratio of confinement stress to the peak unconfined compressive strength of concrete and $\varepsilon_{c0}/\varepsilon_{cc}$ is the ratio of axial strain at the peak strength of unconfined concrete to ultimate axial strain of confined concrete. As shown in Figure 8, assuming that the volume of concrete is unchangeable, then the lateral confining pressure can be calculated by the following equation:

$$f_l = \frac{2f_{BFRP}t_{BFRP}}{D}, \qquad f_{BFRP} = E_{BFRP}\varepsilon_{hoop}, \tag{1}$$

where f_{BFRP} and t_{BFRP} are the hoop tensile strength and the thickness of the BFRP tube, respectively. D is the inner diameter of the tube. E_{BFRP} is the tensile modulus of BFRP and ε_{hoop} is the tensile hoop strain. For the same BFRP tube, the confining pressure of the large-size specimen is 62.5% of that of the small-size one.

Table 2 shows that the peak compression strength of PC is higher than that of CFRC of the small-size specimens. In contrast, the peak strength of CFRC is higher than that of PC of the large-size specimen. Compared with PC, the axial strain of CFRC for both small- and large-size specimens is enhanced due to the bridging effect of the coconut fibers. For all specimens, the confinement of BFRP tubes significantly improves the compressive strength of the concrete. The average compressive strength enhancement f'_{cc}/f'_{c0} of 2L- and 4L-BFRP-PC is 1.48 and 2.20 for small-size specimens, and 1.52 and 2.22 for the large-size specimens, respectively. The average compressive strength enhancement of 2L- and 4L-BFRP-CFRC is 2.15 and 3.03 for the small-size specimens, and 1.22 and 1.63 for the large-size specimens, respectively. As anticipated, the lateral confinement stress f_l increases with the tube thicknesses. The lateral confinement stresses of 2L- and 4L-BFRP-PC for small-size specimens are 2.86 MPa and 5.47 MPa. For the large-size specimens, they are, respectively, 2.63 MPa and 4.25 MPa, respectively, while

Table 1: Test matrix.

Specimens	Number of specimens	Size (mm)	Number of BFRF layers	t_{BFRP} (mm)	Mass (kg)
PC-A	3	100 ∗ 200	0	0	3.79
CFRC-A	3	100 ∗ 200	0	0	3.63
2L-BFRP-RC-A	3	100 ∗ 200	2	1.06	3.85
4L-BFRP-RC-A	3	100 ∗ 200	4	1.57	3.98
2L-BFRP-CFRC-A	3	100 ∗ 200	2	1.04	3.78
4L-BFRP-CFRC-A	3	100 ∗ 200	4	1.58	3.89
PC-B	3	160 ∗ 320	0	0	14.93
CFRC-B	3	160 ∗ 320	0	0	14.75
2L-BFRP-RC-B	3	160 ∗ 320	2	1.05	15.60
4L-BFRP-RC-B	3	160 ∗ 320	4	1.58	15.77
2L-BFRP-CFRC-B	3	160 ∗ 320	2	1.06	15.23
4L-BFRP-CFRC-B	3	160 ∗ 320	4	1.57	15.63

t_{BFRP} is the thickness of the BFRP tube.

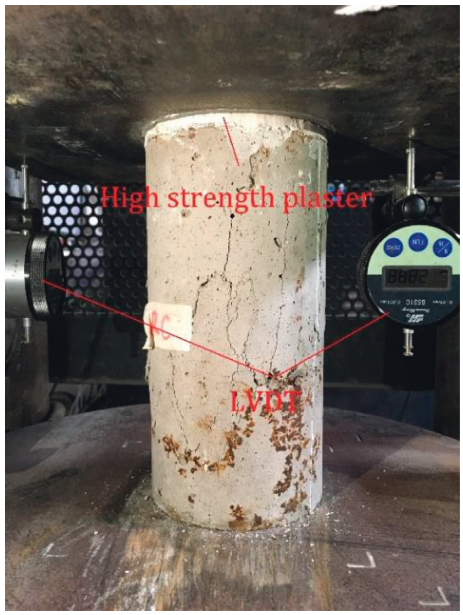

Figure 3: Layout of the compression test.

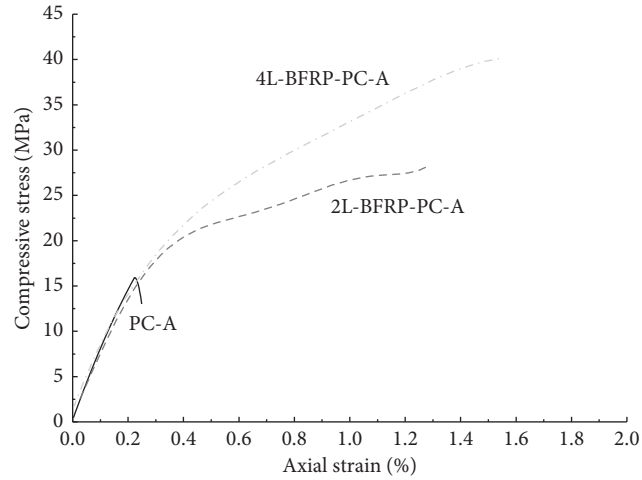

Figure 4: Effect of BFRP layers on the axial stress-strain behavior of the 100 ∗ 200 mm BFRP-PC.

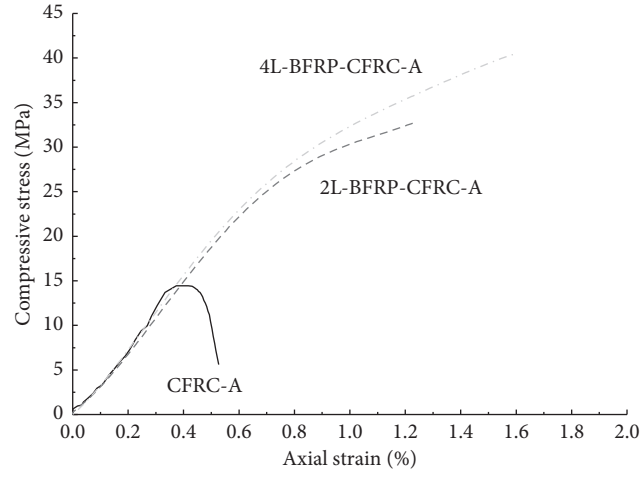

Figure 5: Effect of BFRP layers on the axial stress-strain behavior of the 100 ∗ 200 mm BFRP-CFRC.

the lateral confining pressure of 2L- and 4L-BFRP-CFRC of small-size specimens is 2.92 MPa and 5.99 MPa, and for large-size specimens is 1.30 MPa and 4.02 MPa, respectively. The ultimate axial strain has a similar tendency; that is, the ultimate axial strains of both BFRP-PC and BFRP-CFRC increase with the BFRP tube thicknesses. The ultimate strain reaches 0.013 and 0.0147 for 2L- and 4L-BFRP-PC, and 0.0112 and 0.0154 for 2L- and 4L-BFRP-CFRC for the small-size specimens, respectively. In the case of 2L- and 4L-BFRP-PC, the values are 0.0106 and 0.0136, and in the case of corresponding large-size specimens, they are 0.0112 and 0.0139. Although the compressive strength of unconfined CFRC is lower than that of the unconfined PC, the compression of the BFRP-CFRC specimens is the best due to the joined confinement of coconut fiber and BFRP composite.

3.3. Prediction of Ultimate Compressive Strength. Models for predicting the ultimate compressive strength of concrete cylinder can be divided into two categories, that is, the design-oriented and analysis-oriented models [20]. The design-oriented models have a closed form equation and are

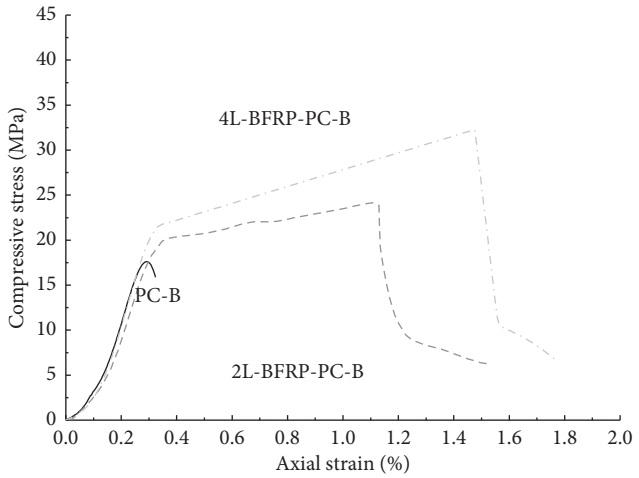

Figure 6: Effect of BFRP layers on the axial stress-strain behavior of the 160 ∗ 320 mm BFRP-PC.

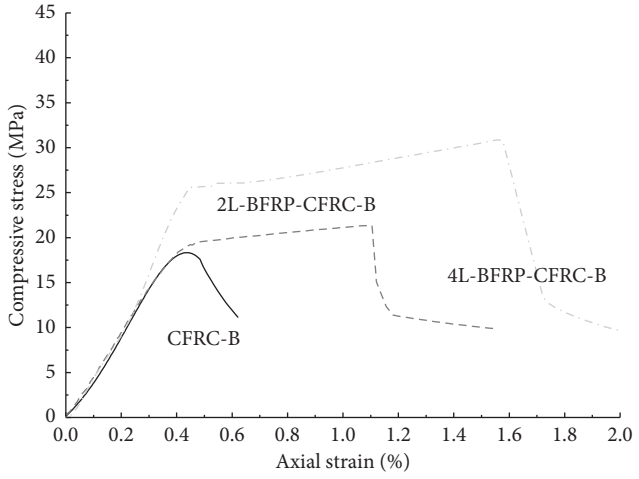

Figure 7: Effect of BFRP layers on the axial stress-strain behavior of the 160 ∗ 320 mm BFRP-CFRC.

directly based on the interpretation of experimental results. These models consider the confined concrete as a single composite material and are thus simple and convenient to apply. The analysis-oriented models are generated using an incremental numerical procedure to predict an increase of the strength. They separately deal with the contribution of confinement and core concrete. The compressive strength prediction is based on the radial displacement compatibility and equilibrium between the confinement and concrete core. In this study, similar approach according to Yan and Chouw [20] is used.

The most common form of design-oriented models can be represented by the following equation:

$$\frac{f'_{cc}}{f'_{c0}} = 1 + k\left(\frac{f_l}{f'_{c0}}\right)^m, \quad (2)$$

where k is the effectiveness coefficient and m is the power coefficient of the confinement ratio. The most frequently used design-oriented models are listed in Table 3. Meanwhile, the often used analysis-oriented models are listed in Table 4. Most of the analysis-oriented models are developed from the Mander [41] model. This model was derived from the William−Warnke failure surface for triaxial compression state with equal effective lateral confining pressure.

Based on those models, the ultimate strength of the specimens is predicted and listed in Tables 5 and 6, respectively.

To verify the prediction precision of each model, the prediction error is defined as

$$\text{error} = \frac{v_{\text{test}} - v_{\text{prediction}}}{v_{\text{test}}}, \quad (3)$$

where v_{test} and $v_{\text{prediction}}$ are the experimental and predicted results, respectively. The summation of the absolute errors of each specimen is used to judge the effectiveness of the model. Design-oriented and analysis-oriented models are listed from the best to the worst, respectively.

Table 5 shows that the predicted ultimate compressive strengths of the BFRP tube-confined specimens are very different. For the small-size specimens, the design-oriented model of Samaan et al. [26] predicted the ultimate compressive strength very well. The errors are, respectively, about 8.24% and −6.91% for the 2L- and 4L-BFRP-PC and −0.61% and −6.35% for the 2L- and 4L-BFRP-CFRC. The model proposed by Toutanji [28] can also precisely predict the ultimate compressive strength. The maximum error is −14.56%. However, some models are not suitable for predicting the compression strength of BFRP-PC/CFRC. The prediction errors are more than 30% compared with the experimental values, such as the models proposed by Wu et al. [24] and Lam and Teng [25], Saafi [27], Karbhari and Gao [29], and Cheng et al. [31]. The analysis-oriented models can somehow better predict the ultimate compressive strength, especially the model proposed by Marques et al. The prediction errors are about 6.58% and −3.95% for the 2L- and 4L-BFRP-PC and −0.99% and 1.38% for the 2L- and 4L-BFRP-CFRC, respectively. The prediction errors of the models proposed by Fam and Rizkalla [32], Saaman et al. [26], Saadatmanesh et al. [33], Restepol and De Vino [34], Spoelstra and Monti [35], and Chun and Park [36], and Binici [38] are within 15%.

In the case of large-size specimens, among the design-oriented models, Lam and Teng's model [23] predicts the compression strength best. The prediction errors are 6.76% and −9.01% for the 2L- and 4L-BFRP-PC, and 0.73% and −17.00% for the 2L- and 4L-BFRP-CFRC, respectively. The model proposed by Teng et al. [40] is the best among the analysis-oriented models, and the prediction errors are 9.25% and −6.22% for the 2L- and 4L-BFRP-PC and 1.87% and −14.98% for the 2L- and 4L-BFRP-CFRC, respectively.

Based on the experimental data in this study, it should be noted that, the prediction precision depends significantly on the size of the specimens. The model proposed by Samaan et al. [26] is the best to predict the ultimate compressive strength of the small-size specimens, but it is the worst to predict the larger ones. In contrast, the model proposed by Marques et al. [39] is the best to predict the ultimate

Table 2: Test results of cylinders.

Specimens	t_{BFRP} (mm)	f'_{c0} (MPa)	ε_{c0} (%)	f'_{cc} (MPa)	ε_{cc} (%)	ε_{hoop} (%)	f_l (MPa)	f'_{cc}/f'_{c0}	f_l/f'_{c0}	$\varepsilon_{cc}/\varepsilon_{c0}$
PC-A	—	15.93	0.21	15.93	0.21	—	—	—	—	—
CFRC-A	—	14.24	0.41	14.24	0.41	—	—	—	—	—
2L-BFRP-RC-A	1.10	15.93	0.21	27.90	1.30	0.99	2.86	1.48	0.15	6.17
4L-BFRP-RC-A	1.75	15.93	0.21	41.43	1.47	1.10	5.47	2.20	0.29	7.01
2L-BFRP-CFRC-A	1.10	14.24	0.30	30.57	1.12	1.01	2.92	2.15	0.21	2.73
4L-BFRP-CFRC-A	1.75	14.24	0.30	43.21	1.54	1.20	5.99	3.03	0.42	3.75
PC-B	—	13.93	0.23	13.93	0.23	—	—	—	—	—
CFRC-B	—	19.09	0.42	19.09	0.42	—	—	—	—	—
2L-BFRP-RC-B	1.09	13.93	0.20	21.23	1.06	1.45	2.63	1.52	0.19	4.59
4L-BFRP-RC-B	1.76	13.93	0.20	30.97	1.36	1.36	4.25	2.22	0.31	5.91
2L-BFRP-CFRC-B	1.08	19.09	0.26	23.33	1.12	0.72	1.30	1.22	0.07	2.67
4L-BFRP-CFRC-B	1.74	19.09	0.26	38.94	1.39	1.29	4.02	1.63	0.21	3.31

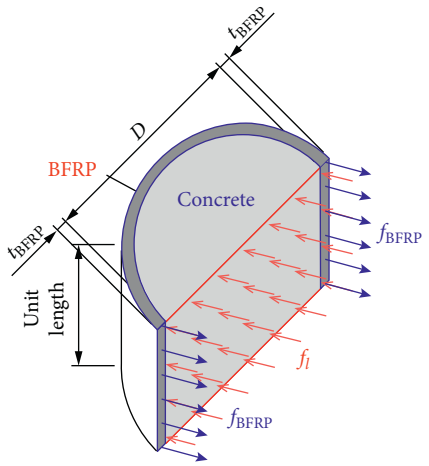

Figure 8: Schematic diagram of the confinement of BFRP tube.

Table 3: Coefficient of design-oriented confinement models.

Models	m	k
Xiao and Wu [21] and Richart et al. [22]	1.0	4.1
Lam and Teng [23]	1.0	3.3
Wu et al. [24] and Lam and Teng [25]	1.0	2.0
Samaan et al. [26]	0.70	3.38
Saafi [27]	0.84	2.2
Toutanji [28]	0.85	3.5
Karbhari and Gao [29]	0.87	2.1
Miyauhi et al. [30]	1.0	2.98
Cheng et al. [31]	1.0	2.4

Table 4: Coefficient of analysis-oriented confinement models.

Models	Equations
Fam and Rizkalla [32], Saaman et al. [26], Saadatmanesh et al. [33], Restepol and De Vino [34], Spoelstra and Monti [35], and Chun and Park [36]	$f'_{cc}/f'_{c0} = 2.254\sqrt{1 + 7.94 f_l/f'_{c0}} - 2 f_l/f'_{c0} - 1.254$
Harries and Kharel [37]	$f'_{cc} = f'_{c0} + 4.629 f_l^{0.587}$
Binici [38]	$f'_{cc} = f'_{c0}(\sqrt{1 + 9.9 f_l/f'_{c0}} + f_l/f'_{c0})$
Marques et al. [39]	$f'_{cc} = f'_{c0} + 6.7 f_l^{0.83}$
Teng et al. [40]	$f'_{cc} = f'_{c0} + 3.5 f_l$

Table 5: Strength prediction of the small-size specimens by design-oriented confinement models.

Models	2L-BFRP-RC (MPa)	Error (%)	4L-BFRP-RC (MPa)	Error (%)	2L-BFRP-CFRC (MPa)	Error (%)	4L-BFRP-CFRC (MPa)	Error (%)
Samaan et al. [26]	30.2	8.24	38.57	−6.91	30.38	−0.61	40.46	−6.35
Toutanji [28]	27.05	−3.06	35.4	−14.56	27.47	−10.15	38.08	−11.87
Xiao and Wu [21] and Richart et al. [22]	25.73	−7.79	34.87	−15.83	26.5	−13.31	38.76	−10.3
Lam and Teng [23]	23.82	−14.64	31.18	−24.75	24.11	−21.14	33.98	−21.37
Miyauhi et al. [30]	23.05	−17.38	29.7	−28.32	23.15	−24.27	32.06	−25.8
Saafi [27]	23.05	−17.38	28.32	−31.65	22.68	−25.79	29.36	−32.06
Karbhari and Gao [29]	22.35	−19.89	27.33	−34.04	21.93	−28.26	28.3	−34.51
Cheng et al. [31]	21.66	−22.35	27.02	−34.79	21.42	−29.94	28.59	−33.83
Wu et al. [24] and Lam and Teng [25]	20.71	−25.77	25.17	−39.25	20.22	−33.85	26.2	−39.36
Marques et al. [39]	29.74	*6.58*	39.79	*−3.95*	30.87	*0.99*	43.81	*1.38*
Binici [38]	27.5	−1.43	35.96	−13.2	27.98	−8.48	38.32	−11.31
Fam and Rizkalla [32], Saaman et al. [26], Saadatmanesh et al. [33], Restepol and De Vino [34], Spoelstra and Monti [35], and Chun and Park [36],	28.39	1.77	36.04	−13.02	28.58	−6.5	37.01	−14.35
Teng et al. [40]	24.29	−12.93	32.1	−22.52	24.71	−19.18	35.17	−18.6
Harries and Kharel [37]	23.65	−15.24	27.3	−34.11	23.05	−24.61	27.47	−36.43

Table 6: Strength prediction of the large-size specimens by design-oriented confinement models.

Models	2L-BFRP-RC (MPa)	Error (%)	4L-BFRP-RC (MPa)	Error (%)	2L-BFRP-CFRC (MPa)	Error (%)	4L-BFRP-CFRC (MPa)	Error (%)
Xiao and Wu [21] and Richart et al. [22]	24.78	16.73	31.64	2.15	24.57	5.31	35.53	−8.77
Lam and Teng [23]	22.66	6.76	28.18	−9.01	23.5	0.73	32.32	−17
Miyauhi et al. [30]	21.82	2.77	26.8	−13.47	23.07	−1.11	31.04	−20.3
Toutanji [28]	25.81	21.59	31.95	3.15	26.06	11.7	36.82	−5.44
Saafi [27]	21.52	1.39	25.39	−18.02	23.59	1.11	30.41	−21.9
Karbhari and Gao [29]	20.83	−1.9	24.49	−20.92	23.06	−1.18	29.4	−24.49
Cheng et al. [31]	20.28	−4.47	24.29	−21.56	22.3	−4.43	28.71	−26.27
Wu et al. [24] and Lam and Teng [25]	19.22	−9.45	22.57	−27.13	21.76	−6.72	27.11	−30.39
Samaan et al. [26]	28.65	34.96	34.67	11.95	29.12	24.82	40.73	4.6
Teng et al. [40]	23.19	9.25	29.04	−6.22	23.77	1.87	33.12	−14.94
Binici [38]	26.29	23.84	32.42	4.67	26.18	12.2	37.51	−3.68
Fam and Rizkalla [32], Saaman et al. [26], Saadatmanesh et al. [33], Restepol and De Vino [34], Spoelstra and Monti [35], and Chun and Park [36],	26.97	27.03	32.31	4.33	27.06	15.98	38.32	−1.6
Harries and Kharel [37]	22.13	4.22	24.85	−19.75	24.58	5.35	29.55	−24.12
Marques et al. [39]	28.96	36.4	36.49	17.83	27.61	18.36	40.3	3.5

compressive strength of large-size specimens, but it is the worst to predict the smaller ones.

3.4. Prediction of Ultimate Axial Strain. The most frequently used models to predict the ultimate axial strain are listed in Table 7. Based on those models, the ultimate strains of small-size specimens and large-size specimens are predicted and listed in Tables 8 and 9, respectively. The error of all 4 specimens is used to evaluate the effectiveness of the model and is listed in the best to the worst order. Tables 8 and 9 show that the model proposed by Miyauchi et al. [30] fits the experimental ultimate strains very well for all specimens considered. For the small-size specimens, the errors are about 0.62% and 7.12% for the 2L- and 4L-BFRP-PC, and 21.41% and 9.57% for the 2L- and 4L-BFRP-CFRC,

Table 7: Prediction models of the ultimate axial strain.

Models	Equations
Wu et al. [24]	$\varepsilon_{cc} = \varepsilon_{c0}(1.3 + 6.3f'_{cc}/f'_{c0})$
Fam and Rizkalla [32], Saaman et al. [26], Saadatmanesh et al. [33], Restepol and De Vino [34], Spoelstra and Monti [35], and Chun and Park [36], Harries and Kharel [37], Binici [38], Marques et al. [39], Teng et al. [40], and Mander et al. [41]	$\varepsilon_{cc} = \varepsilon_{c0}[1.0 + 5.0(f'_{cc}/f'_{c0} - 1)]$
Richart et al. [22]	$\varepsilon_{cc} = 0.002 + 0.001E_{FRP}t_{FRP}/Df'_{c0}$
Saafi [27]	$\varepsilon_{cc} = \varepsilon_{c0}[1.0 + (537\varepsilon_{FRP} + 2.6)(f'_{cc}/f'_{c0} - 1)]$
Miyauchi et al. [30]	$\varepsilon_{cc} = 0.002[1.0 + 10.6(2t_{FRP}f_{FRP}/Df'_{c0})^{0.373}]$
Lam and Teng for GFRP tube [42]	$\varepsilon_{cc}/\varepsilon_{c0} = 2.0 + 27.0(f'_{cc}/f'_{c0})^{0.7}$
Lam and Teng for CFRP sheet [42]	$\varepsilon_{cc}/\varepsilon_{c0} = 2.0 + 15.0(f'_{cc}/f'_{c0})$

Table 8: Ultimate axial strain prediction of the small-size specimens (units: %).

Models	2L-BFRP-RC	Error	4L-BFRP-RC	Error	2L-BFRP-CFRC	Error	4L-BFRP-CFRC	Error
Miyauchi et al. [30]	1.30	0.62	1.58	7.12	1.36	21.41	1.68	9.57
Richart et al. [22]	1.09	−16.0	1.64	11.35	1.39	24.34	2.01	30.77
Fam and Rizkalla [32], Saaman et al. [26], Saadatmanesh et al. [33], Restepol and De Vino [34], Spoelstra and Monti [35], and Chun and Park [36], Harries and Kharel [37], Binici [38], Marques et al. [39], Teng et al. [40], and Mander et al. [41]	0.71	−44.9	1.47	−0.14	2.77	147.10	4.57	197.62
Saafi [27]	1.01	−22.2	2.35	59.9	4.19	274.39	7.94	416.75
Wu et al. [24]	2.23	72.2	3.18	116.3	6.09	443.43	8.36	444.24
Lam and Teng for CFRP sheet [42]	5.08	292.1	7.35	399.3	14.04	1153.79	19.45	1166.57
Lam and Teng for GFRP tube [42]	7.88	508.1	10.27	597.4	19.74	1662.24	24.87	1519.29
ε_{max}	1.93	49.09	2.14	45.46	1.97	75.92	2.33	51.70

Table 9: Ultimate axial strain prediction of the large-size specimens (units: %).

Models	2L-BFRP-RC	Error	4L-BFRP-RC	Error	2L-BFRP-CFRC	Error	4L-BFRP-CFRC	Error
Miyauchi et al. [30]	1.32	25.29	1.51	11.38	0.97	−13.48	1.35	−3.29
Fam and Rizkalla [32], Saaman et al. [26], Saadatmanesh et al. [33], Restepol and De Vino [34], Spoelstra and Monti [35], and Chun and Park [36], Harries and Kharel [37], Binici [38], Marques et al. [39], Teng et al. [40], and Mander et al. [41]	0.72	−31.82	1.42	4.41	0.88	−21.60	1.17	−16.28
Richart et al. [22]	0.83	−21.61	1.22	−10.19	1.74	55.63	2.60	87.07
Saafi [27]	1.28	21.23	2.62	92.38	2.13	90.27	4.58	229.13
Wu et al. [24]	2.18	105.98	3.06	124.79	4.86	333.84	5.94	327.00
Lam and Teng for CFRP sheet [42]	4.96	369.70	7.06	419.12	11.11	891.88	13.69	883.62
Lam and Teng for GFRP tube [42]	7.64	623.40	9.84	623.32	16.80	1400.37	19.52	1302.23
ε_{max}	0.0280	165.02	2.63	93.43	1.41	26.30	2.50	79.56

respectively. For the large-size specimens, they are 25.29% and 11.38% for the 2L- and 4L-BFRP-PC, and −13.48% and −3.29% for the 2L- and 4L-BFRP-CFRC, respectively. However, most of the other models overestimate the ultimate axial strains of the specimens.

To evaluate the effectiveness, it is assumed that (1) there is no gap between the tube and concrete, and the expansion of the concrete can directly transverse to the confinement of the BFRP tube; (2) the volume increase due to the cracks created during the compression process is ignored; and (3) BFRP tube experiences homogeneous expansion in the hoop direction. Based on these assumptions, the maximum ultimate axial strain of the concrete can be obtained:

$$\frac{1}{4}\pi D^2 H = \frac{1}{4}\pi (D + \Delta D)^2 (H - \Delta H), \quad (4)$$

$$\Delta D = D\varepsilon_{\text{hoop}}, \quad (5)$$

$$\varepsilon_{cc}' = \ln\left(1 + \frac{\Delta H}{H}\right) = \ln\left[2 - \frac{1}{\left(1 + \varepsilon_{\text{hoop}}\right)^2}\right], \quad (6)$$

where D is the inner diameter of the tube, H is the height of the specimen, ΔD is the expansion of the specimen during compression, ΔH is the compression deformation of the concrete, and ε_{cc}' is the maximum ultimate axial strain of the concrete. Equation (6) is almost a straight line for $\varepsilon_{\text{hoop}}$ between 0 and 0.1; that is, ε_{cc}' increases linearly with $\varepsilon_{\text{hoop}}$. The maximum ultimate axial strains ε_{max} can be gotten when the tube is fractured in the hoop direction. ε_{max} are listed in the last row of Tables 8 and 9. Because the fracture strain of the BFRP tube in the hoop direction is significantly smaller than the results of the coupon tests, the models proposed by Lam and Teng [42] significantly overestimate the ultimate axial strain ε_{max} of the concrete specimens.

4. Conclusions

The axial compressive behavior of BFRP tube-confined PC and CFRC are investigated. In total, 36 compressive tests were carried out to reveal the effects of the BFRP tube thickness, the specimen size, and the coconut fibers inclusion on the ultimate axial compressive strength and strain. The results reveal the following:

(i) BFRP tube confinement enhanced the compressive strength and ductility of both PC and CFRC.

(ii) The accuracy of the compressive strength prediction depends on the size of the specimens. The model proposed by Samaan et al. [26] provides the best estimate of the ultimate compressive strength of small-size specimens. However, among the 9 design-oriented models considered, it gives the worst prediction of the value for larger specimens.

(iii) The model proposed by Miyauchi et al. [30] fits the experimental ultimate strains very well for both small- and large-size specimens.

(iv) An inclusion of coconut fiber can significantly increase the ductility of the specimens.

Data Availability

The data used to support the findings of this study are available from the corresponding author upon request.

Conflicts of Interest

The authors declare that they have no conflicts of interest.

Acknowledgments

The authors gratefully acknowledge the partial support of this research by the National Key Research and Development Program of China under Grant no. 2016YFC0701100, the National Natural Science Foundation of China under Grant no. 51508373, and the Tianjin Basic Research Program under Grant nos. 16JCZDJC38900 and 15JCZDJC39900.

References

[1] L. B. Yan, N Chouw, and K. Jayaraman, "Flax fibre and its composites—a review," *Composites Part B: Engineering*, vol. 56, pp. 296–317, 2014.

[2] J. Reis, "Fracture and flexural characterization of natural fibre-reinforced polymer concrete," *Construction and Building Materials*, vol. 20, pp. 673–678, 2006.

[3] P. Baruah and S. Talukdar, "A comparative study of compressive, flexural, tensile and shear strength of concrete with fibres of different origins," *Indian Concrete Journal*, vol. 81, pp. 17–24, 2007.

[4] S. M. Islam, R. R. Hussain, and M. A. Z. Morshed, "Fiber-reinforced concrete incorporating locally available natural fibers in normal-and high-strength concrete and a performance analysis with steel fiber-reinforced composite concrete," *Journal of Composite Materials*, vol. 46, no. 1, pp. 111–122, 2012.

[5] N. M. S. Hasan, H. R. Sobuz, M. S. Sayed, and S. M. Islam, "The use of coconut fibre in the production of structural lightweight concrete," *Journal of Applied Science*, vol. 12, no. 9, pp. 831–839, 2012.

[6] M. Ali, A. Liu, H. Sou, and N. Chouw, "Mechanical and dynamic properties of coconut fibre reinforced concrete," *Construction and Building Materials*, vol. 30, pp. 814–825, 2012.

[7] J. Sim, C. Park, and D. Y. Moon, "Characteristics of basalt fiber as a strengthening material for concrete structures," *Composites Part B: Engineering*, vol. 36, no. 6-7, pp. 504–12, 2005.

[8] J. M. Park, W. G. Shin, and D. J. Yoon, "A study of interfacial aspects of epoxy-based composites reinforced with dual basalt and SiC fibres by means of the fragmentation and acoustic emission techniques," *Composites Science and Technology*, vol. 59, no. 3, pp. 355–70, 1999.

[9] S. Matko, P. Anna, G. Marosi et al., "Use of reactive surfactants in basalt fiber reinforced polypropylene composites," *Macromolecular Symposia*, vol. 202, no. 1, pp. 255–68, 2003.

[10] T. Czigány, "Basalt fiber reinforced hybrid polymer composites," *Materials Science Forum*, vol. 473-474, pp. 59–66, 2005.

[11] P. I. Bashtannik, V. G. Ovcharenko, and Y. A. Boot, "Effect of combined extrusion parameters on mechanical properties of basalt fiber-reinforced plastics based on polypropylene," *Mechanics of Composite Materials*, vol. 33, no. 6, pp. 600–603, 1997.

[12] S. Öztürk, "The effect of fibre content on the mechanical properties of hemp and basalt fibre reinforced phenol formaldehyde composites," *Journal of Materials Science*, vol. 40, no. 17, pp. 4585–4592, 2005.

[13] S. E. Artemenko, "Polymer composite materials made from carbon, basalt, and glass fibres. Structure and properties," *Fibre Chemistry*, vol. 35, no. 3, pp. 226–229, 2003.

[14] V. Lopresto, C. Leone, and I. De Iorio, "Mechanical characterisation of basalt fibre reinforced plastic," *Composites Part B: Engineering*, vol. 42, no. 4, pp. 717–723, 2011.

[15] G. Wu, X. Wang, Z. Wu, Z. Dong, and G. Zhang, "Durability of basalt fibers and composites in corrosive environments," *Journal of Composite Materials*, vol. 49, no. 7, pp. 873–887, 2014.

[16] Z. Wu, X. Wang, K. Iwashita, T. Sasaki, and Y. Hamaguchi, "Tensile fatigue behaviour of FRP and hybrid FRP sheets," *Composites Part B: Engineering*, vol. 41, no. 5, pp. 396–402, 2010.

[17] C. Colombo, L. Vergani, and M. Burman, "Static and fatigue characterisation of new basalt fibre reinforced composites," *Composite Structures*, vol. 94, no. 3, pp. 1165–1174, 2012.

[18] W. S. Chen, H. Hao, M. Jong et al., "Quasi-static and dynamic tensile properties of basalt fibre reinforced polymer," *Composites Part B: Engineering*, vol. 125, pp. 123–133, 2017.

[19] L. Yan, F Dong, N Chouw, and K. Jayaraman, "Seismic performance of flax FRP encased coconut fibre reinforced concrete column," in *Proceedings of the 2013 Australian Earthquake Engineering Society Conference*, pp. 15–17, Hobart, Australia, November 2013.

[20] LB Yan and N Chouw, "Behavior and analytical modeling of natural flax fibre reinforced polymer tube confined plain concrete and coir fibre reinforced concrete," *Journal of Composite Materials*, vol. 47, no. 17, pp. 2133–2148, 2013.

[21] Y Xiao and H Wu, "Compressive behaviour of concrete confined by carbon fiber composites jackets," *Journal of Materials in Civil Engineering*, vol. 12, no. 2, pp. 139–146, 2000.

[22] F. E. Richart, A. Brandtzaeg, and R. L. Brown, *A Study of the Failure of Concrete under Combined Compressive Stresses*, University of Illinois. Engineering Experimental Station, Champaign, IL, USA, 1928.

[23] L. Lam and J. G. Teng, "Design-oriented stress–strain model for FRP-confined concrete," *Construction and Building Materials*, vol. 17, no. 6-7, pp. 471–489, 2003.

[24] G. Wu, Z. T. Lu, and Z. S. Wu, "Strength and ductility of concrete cylinders confined with FRP composites," *Construction and Building Materials*, vol. 20, no. 3, pp. 134–148, 2006.

[25] L. Lam and J. G. Teng, "Strength models for fiber-reinforced plastic-confined concrete," *ASCE Journal of Structural Engineering*, vol. 128, no. 5, pp. 612–623, 2002.

[26] M. Samaan, A. Mirmiran, and M. Shahawy, "Model of concrete confined by fibre composites. Strength models for fiber-reinforced plastic-confined concrete," *ASCE Journal of Structural Engineering*, vol. 124, no. 9, pp. 1025–1031, 1998.

[27] M. Saafi, "Design and fabrication of FRP grids for aerospace and civil engineering applications," *Journal of Aerospace Engineering*, vol. 13, no. 4, pp. 144–149, 2000.

[28] H. A. Toutanji, "Stress–strain characteristics of concrete columns externally confined with advanced fiber composite sheets," *ACI Materials Journal*, vol. 96, no. 3, pp. 397–404, 1998.

[29] V. M. Karbhari and Y. Gao, "Composite jacketed concrete under uniaxial compression-verification of simple design equations," *Journal of Materials in Civil Engineering*, vol. 9, no. 4, pp. 185–193, 1997.

[30] K. Miyauchi, S. Inoue, T. Kuroda et al., "Strengthening effects of concrete columns with carbon fibre sheet," *Proceeding of Japanese Concrete Institute*, vol. 21, no. 3, pp. 1453–1458, 1999.

[31] H. L. Cheng, E. D. Sotelino, and W. F. Chen, "Strength estimation for FRP wrapped reinforced concrete columns," *Steel and Composite Structures*, vol. 2, no. 1, pp. 1–20, 2002.

[32] A. Fam and S. H. Rizkalla, "Confinement model for axially loaded concrete confined by circular fibre-reinforced polymer tube," *ACI Structural Journal*, vol. 98, no. 4, pp. 451–461, 2001.

[33] H. Saadatmanesh, M. R. Ehasni, and M. W. Li, "Strength and ductility of concrete columns externally reinforced with fibre composites straps," *ACI Structural Journal*, vol. 91, no. 4, pp. 434–447, 1994.

[34] J. I. Restrepol and B. De Vino, "Enhancement of the axial-loadapacity of reinforced concrete columns by means of fibre glass-epoxy jacket," in *Proceedings Second International Conference on Advanced Composite Materials in Bridges and Structures*. M. M. EI-ardy, Ed., pp. 547–553, Montreal, Canada, 1996.

[35] M. R Spoelstra and G. Monti, "FRP-confined concrete model," *ASCE Journal of Composites for Construction*, vol. 3, no. 3, pp. 143–150, 1999.

[36] S. S. Chun and H. C. Park, "Load carrying capacity and ductility of RC columns confined by carbon fibre reinforced polymer," in *Proceedings of Third International Conference on Composites in Infrastructure*, San Francisco, CA, USA, 2002.

[37] K. A. Harries and G. Kharel, "Behaviour and modeling of concrete subjected to variable confining pressure," *ACI Material Journal*, vol. 99, no. 2, pp. 180–189, 2002.

[38] B. Binici, "An analytical model for stress-strain behavior of confined concrete," *Engineering Structures*, vol. 27, no. 7, pp. 1040–1051, 2005.

[39] S. P. C. Marques, D. C. S. C. Marques, J. L. da Silva, and M. A. A. Cavalcante, "Model for analysis of short columns of concrete confined by fibre-reinforced polymer," *ASCE Journal of Composites for Construction*, vol. 8, no. 4, pp. 332–340, 2004.

[40] J. G. Teng, Y. L. Huang, L. Lam, and L. P. Ye, "Theoretical model for fibre reinforced polymer-confined concrete," *ASCE Journal of Composites for Construction*, vol. 11, no. 2, pp. 201–211, 2007.

[41] J. B. Mander, M. J. N. Priestley, and R. Park, "Theoretical stress-strain model for confined concrete," *ASCE Journal of Structural Engineering*, vol. 114, no. 8, pp. 1804–1826, 1998.

[42] L. Lam and J. G. Teng, "A new stress-train model for FRP confined concrete," in *Proceedings of the International Conference on FRP Composite in Civil Engineer*, J. G. Teng, Ed., pp. 283–292, Hong Kong, China, December 2001.